Nano Res (2008) 1: 166–175
DOI 10.1007/s12274-008-8010-y
Research Article

Nanotubes in a Gradient Electric Field as Revealed by STM–TEM Technique

Dmitri Golberg[1, 2] (✉), Pedro M. F. J. Costa[1, 3] (✉), Masanori Mitome[1], and Yoshio Bando[2]

[1] Nanoscale Materials Center, Namiki 1-1, Tsukuba, Ibaraki 305-0044, Japan
[2] International Center for Materials Nanoarchitectonics (MANA), National Institute for Materials Science, Namiki 1-1, Tsukuba, Ibaraki 305-0044, Japan
[3] Center for Research in Ceramics and Composite Materials, University of Aveiro, 3810-193 Aveiro, Portugal

Received: 25 April 2008 / Revised: 4 June 2008 / Accepted: 4 June 2008

ABSTRACT

We have investigated the behavior of two nanotube systems, carbon and boron nitride, under controlled applied voltages in a high-resolution transmission electron microscope (TEM) equipped with a scanning tunneling microscope (STM) unit. Individual nanotubes (or thin bundles) were positioned between a piezo-movable gold electrode and a biased (up to ±140 V) STM tip inside the pole-piece of the microscope. The structures studied include double- and multi-walled carbon nanotubes (the latter having diverse morphologies due to the various synthetic procedures utilized), few-layered boron nitride nanotube bundles and multi-walled boron nitride nanotubes (with or without functionalized surfaces). The electrical breakdown, physical failure, and electrostatic interactions are documented for each system.

KEYWORDS

Carbon nanotubes, boron nitride nanotubes, transmission electron microscope, scanning tunneling microscope

Introduction

One of the most exciting and promising applications of nanotube is in the field of nanoelectronics and many papers have recently appeared dealing with the electrical performance of nanotubes in interconnectors, current rectifiers, field-effect transistors, and other devices [1, 2]. These measurements have been performed primarily with instruments, such as scanning electron microscopes (SEM) and atomic force microscopes (AFM) in such a way which affords no access to the internal structure of the nanotube. Furthermore, temporal and spatial-resolution limitations have impaired the observation of changes/alternations during the device performance. At present, knowledge of the limits of nanotube functioning at moderate and relatively high voltages and current densities, which is of prime importance in terms of their efficient integration in nanocircuits, is rather uncertain; failure of a nanotube might strongly depend on its structural features and chemistry, such as the state of ordering of the tubular layers, their number, the tube diameter, and the existence of defects, dopants, or functional groups. Electrical property measurements under time-resolved high spatial- and chemical-resolution, as accessible using a transmission electron microscope (TEM), have only recently started to attract full attention [3–16].

Address correspondence to Dmitri Golberg, golberg.dmitri@nims.go.jp; Pedro M. F. J. Costa, pedromfjcosta@ua.pt

In order to perform such studies, it is necessary to design special types of TEM holders with integrated scanning tunneling microscope (STM) units [4].

In the present contribution, we analyze the behavior of nanotubes with various morphologies, structures, and compositions when subjected to a gradient electric field generated through biasing of an STM tip (up to tens of volts) inside a high-resolution TEM (HRTEM). In particular, the two main nanotube systems—carbon and boron nitride—have been selected and thoroughly compared. Six different nanotube systems having a variety of morphologies, geometries, and states of ordering were examined: (1) double-walled carbon nanotube bundles produced using a chemical vapor deposition (CVD) route [17]; (2) well-structured multi-walled carbon nanotubes prepared via a standard arc-discharge technique [18]; (3) fairly disordered turbostratic-like carbon herringbone fibers fabricated through plasma-enhanced CVD [19]; (4) few-walled (mainly double-walled) boron nitride nanotube bundles synthesized through a substitution reaction from carbon nanotube templates [20]; (5) well-structured multi-walled boron nitride nanotubes fabricated by a floating catalyst induction-heating method [21]; and (6) multi-walled boron nitride nanotubes functionalized with organic moieties [22]. The results for all six systems are illustrated below and compared.

1. Experimental

Previously reported procedures were employed to prepare the carbon [17–19] and boron nitride [20–22] nanotubes. The electrical measurements were carried out by means of a Nanofactory Instruments AB STM integrated holder for TEM shown in Fig. 1. This was used in a field-emission high-resolution JEOL JEM-3100FEF TEM operated at 300 kV. In order to mount a nanotube sample, a fresh-cut gold wire (0.25 mm in diameter) was first inserted into the micro-hole of a removable gold hat attached to the grounded part of the holder. The gold wire tip protruding from the hat was then delicately immersed into the nanotube powder. The hat was finally placed on the sapphire ball of the piezo-driven tube (Fig. 1(b)). It should be noted that the nanotubes were attached to the gold wires simply due to adhesion forces, as shown in Fig. 1(a). No organic glues or pastes were used, in order to avoid contamination of the electrical circuit. After the gold hat had been fixed on the sapphire ball, the sample wire position was adjusted relative to the counter electrode, a sharply etched STM gold tip, as shown in Fig. 1(b). With the help of an optical microscope and through manual manipulation with tweezers, the minimum possible gap between the two metallic contacts was achieved. The holder was then carefully inserted into the TEM. The microscope was equipped with an electron energy loss spectrometer (EELS, Omega filter) and an energy dispersion X-ray detector (EDS, Noran). Therefore, precise structural and chemical analysis of the nanotube samples before, during, and after manipulation/deformation/electrical probing could be performed in situ by parallel TEM imaging, electron diffraction, and

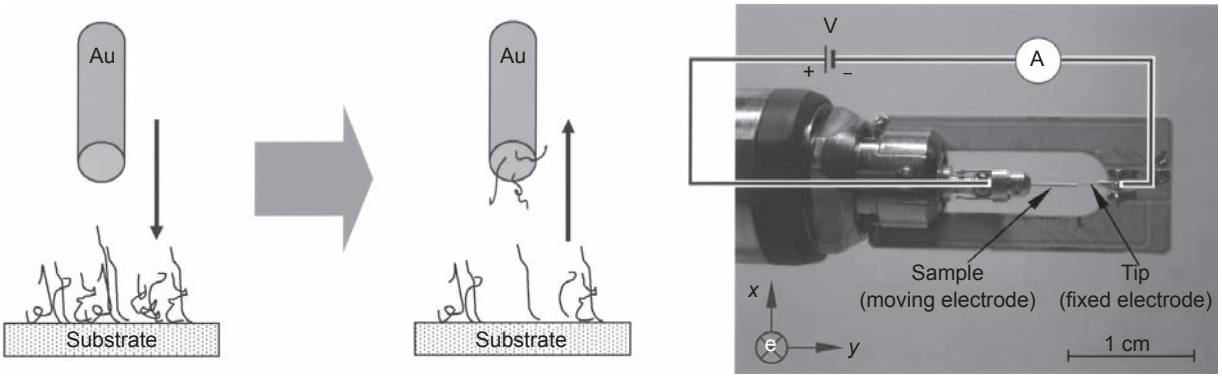

Figure 1 (a) Sketch illustrating the procedure of nanotube sample loading on the gold electrode; and (b) set-up of the TEM–STM holder with the main parts highlighted

spatially-resolved spectroscopic methods. Inside the TEM, the relative *z*-heights of the STM gold tip and the nanotube objects were finely adjusted using the TEM wobbler function. Physical contact between the nanotubes and the STM probe was accomplished by means of subtle piezo-movements of the sample wire (with a precision better than 1 nm) with continuous TEM imaging. The sharp STM gold tip was biased up to ±140 V, the limit of the present experimental set-up. The current transport experiments were executed in three modes: (1) a fast (typically, within a 100–200 ms range) reverse-forward bias sweeping regime with a voltage window chosen relative to the nanotube conductance; (2) a slow, unidirectional increase of bias (reverse or forward) until noticeable morphological changes started to occur in the nanostructure (this allowed the structural failure to be recorded); and (3) setting of a bias which was known to cause initial traces of structural modulations and subsequently keeping it unchanged over time (typically dozens of minutes), while observing and recording (30 frames per second) the complete structural failure with a TV camera.

2. Results

2.1 Carbon nanotubes

2.1.1 *Double-walled CVD-grown carbon nanotubes*

Figure 2 shows a bunch of double-walled carbon nanotubes placed between the gold STM tip, which was biased during the experiment, and the gold sample wire. Initially the bunch displayed nonlinear *I*–*V* curves and an estimated resistance of ~7.5 MΩ. This high figure can be mainly attributed to poor physical contact between the electrodes and the nanotube surface. Accordingly, lower resistances (~1.7 MΩ) were obtained after delicate pressing of the bundles toward the tip which significantly improved the contact. This action, however, did not change the shape of the *I*–*V* curve which remained nonlinear. Next, a study of the stability of the bundles to high current flows was carried out under the continuous increase of bias voltage, as shown in Fig. 2(b). During this process the bundles gradually started to unravel culminating, after reaching a bias of ~9 V after 19 min, in the formation of a single-bundle bridge between the two gold contacts. At this point, the bias was stabilized at +9.2 V with the purpose of following any morphological transformations taking place in the system. The bundle was quite resilient with no major changes seen to be occurring after 2 min under the high current flow. This led to the impromptu testing of its mechanical resistance by slowly driving the anode away, effectively stretching the bundle. It took approximately 7 min to induce the complete collapse of the bundle, which stretched to a maximum of three times its initial length before breaking (Fig. 2(b), inset). HRTEM, albeit difficult to observe due to mechanical instabilities and drifting of the now free-

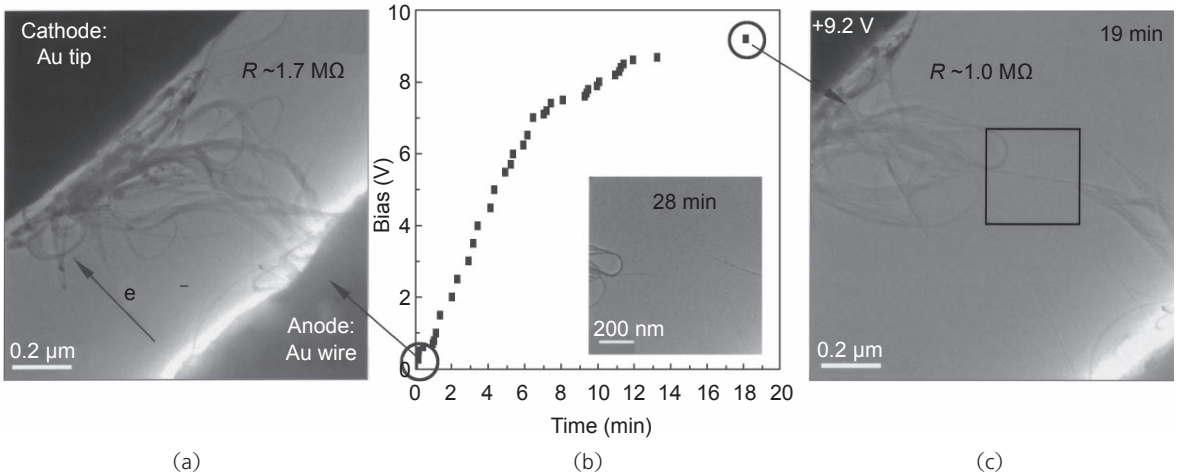

Figure 2 TEM images of a bunch of CVD-synthesized double-walled carbon nanotubes stretched between a gold tip and a gold sample wire before (a) and after (c) tip biasing. The plot of bias increase with time is shown in (b); the circles indicate the stages shown in (a) and (c); the inset in (b) displays a single nanotube bundle broken after 28 min at +9.2 V

standing bundle ends, revealed that the tips still consisted of several thin tubes, rather than individual nanostructures (see Electronic Supplementary Material, Fig. S-1). This allowed the generation of a new contact using one of the protruding bundles. The initial *I*–*V* curve obtained was nonlinear with an estimated resistance of ~1.7 MΩ, which is similar to that of the large bunch. Tightening the contact, again through gentle manipulation, resulted in the alteration of not only the magnitude, but also the shape of the *I*–*V* curve. The character of the system was Ohmic with a calculated resistance of the order of 0.5 –1 MΩ.

2.1.2 *Arc-discharge individual multi-walled carbon nanotubes*

Figure 3 shows an individual perfectly-structured multi-walled carbon nanotube connected to the gold tip and bent in order to improve the quality of the nanotube-electrode contact (Fig. 3(a), inset). Generally, these nanotubes had a metallic-like behavior with linear *I*–*V* curves and total resistances in the range of several hundreds of kilohms. It should be noted that the presence of the amorphous layer covering the surface of the electrode did not influence the shape of the *I*–*V* curves or the high-current flow experiments. This layer, with a thickness of 3–10 nm and therefore visible only at high resolution, was seen throughout the experiments and arises from unavoidable organic contamination during the preparation of the etched Au tip electrode. Its presence may, however, increase the potential barrier and alter the absolute values of the contact resistance. After biasing the electrode to several volts, gradual changes were initiated in the outermost layers of the tube, as shown in Fig. 3(b). The layers were consumed in a layer-by-layer fashion (layer-stripping) leading to visible thinning of the nanotube close to its middle part. Interestingly, the structure of the tubular graphene sheets did not change sinces the remaining layers retained their crystalline arrangement. Furthermore, the extracted resistances were also of similar magnitude implying that the exact number of layers is not very important. An extended stripping process, requiring several tens of minutes and relatively high voltages of +8–10 V inevitably resulted in failure of the nanotube.

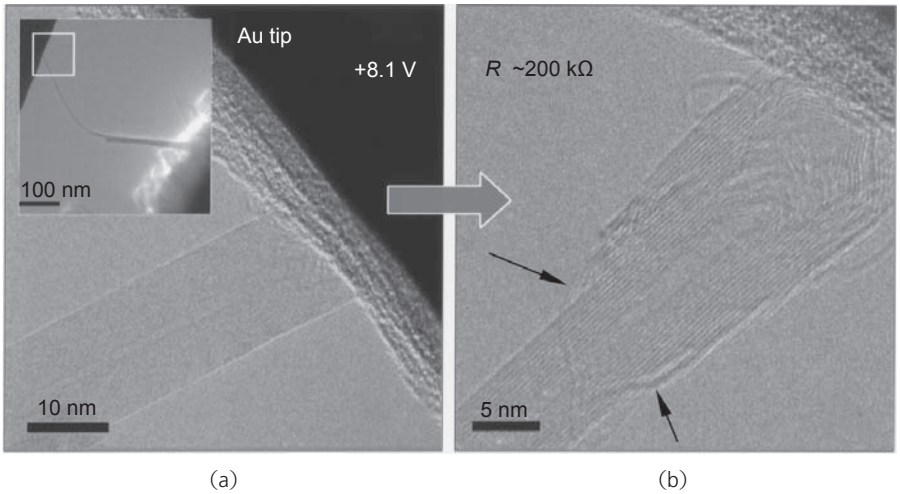

Figure 3 TEM images of an individual arc-discharge-produced and perfectly-structured multi-walled carbon nanotube at the initial (a) and intermediate (b) stages of biasing (after applying a +8.1 V bias to the gold tip for 28 min). The inset depicts a low-magnification TEM image of the initial tube. The arrows in (b) point at damaged external nanotube domains close to the biased electrode

2.1.3 *Plasma-enhanced CVD-grown carbon herringbone fibers*

Figure 4 displays an individual poorly-structured carbon fiber containing a catalytic Fe–Ni particle and connected to the gold electrode. The contact is made entirely through the carbon shell since this completely envelops the metal alloy, as verified through HRTEM imaging. Highly-disordered graphitic layers, organized in a turbostratic-like fashion, were characteristic of this particular system in stark contrast to the structural order seen for the previous two carbon nanotube types. In the first acquisition, these type of fibers revealed linear *I*–*V* curves with resistances in the range of several hundreds of kilohms. After biasing the gold electrode to several volts, significant changes resulted. The first to be noticed was the appearance (or enlargement) of a hollow tubular core along the fiber length. Concomitantly to this, the herringbone structure rearranged into a stack of conically shaped

layers, possibly due to graphitization of the turbostratic layers. Subsequently, at approximately its mid-length, the fiber started to burn in a manner resembling that of the arc-discharge carbon nanotubes. Accordingly, fiber thinning occured by continued burning of its external fragments as a result of Joule heating of the whole structure. The consecutive sublimation of disordered turbostratic-like layers from the outside inwards resulted in complete fiber failure after several minutes and at +7.1 V bias, with its filled tip seen to remain in place. Despite variations in rupture voltage (from 4 to 7 V), the morphological changes were consistent for all fibers studied and independent of the presence of catalyst particles (see Electronic Supplementary Material, Fig. S-2). HRTEM of the broken ends of the fiber, Fig. 4(f), revealed the presence of a single highly folded graphitic sheet which can be thought of as a corrugated graphene layer.

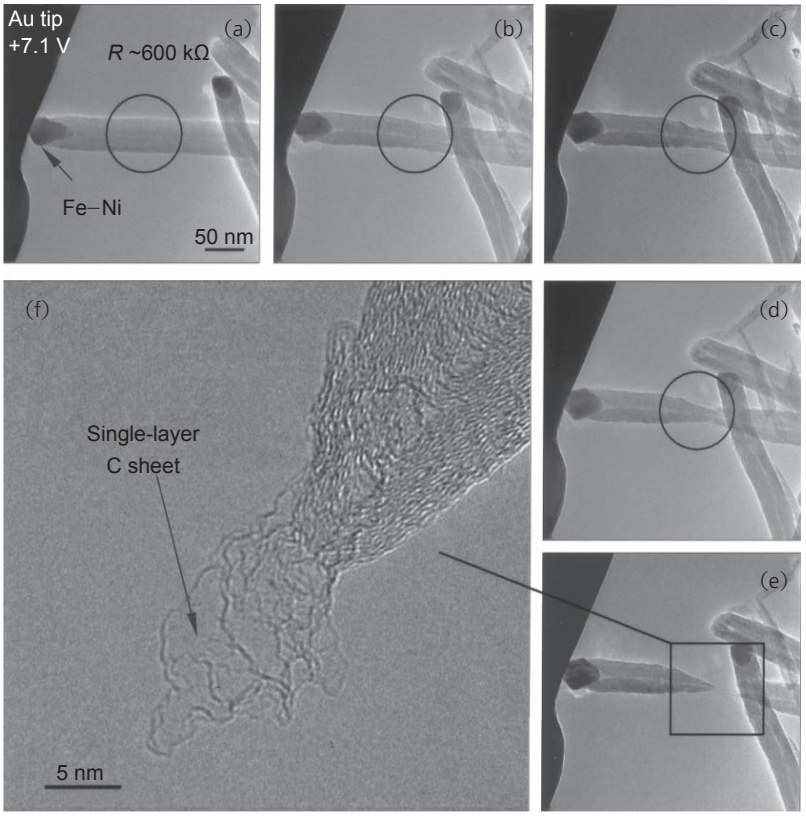

Figure 4 Consecutive TEM images (a)–(e) demonstrating the gradual thinning of a plasma-enhanced-CVD-produced carbon fiber under a +7.1-V bias on a gold tip. The fiber consumption occurs in the inward direction, i.e., towards its core. Complete burning takes place at its mid-length after ~25 min. The failure results in the appearance of a folded graphene sheet at the burned fiber end (f)

2.2 Boron nitride nanotubes

2.2.1 *Thin bundles of few-layered (typically two) boron nitride nanotubes*

Figure 5 depicts TEM images of several boron nitride nanotube bundles positioned between the two gold electrodes. Even up to very high-voltages of ±140 V (the limit of the present experimental set-up) the bundles do not allow a measurable current to pass, thus revealing a perfect dielectric behavior with an estimated resistance of over 10 GΩ. With increasing bias voltage, the strong electrostatic interactions between the positively charged boron nitride structures (a consequence of the 300 kV TEM electron beam) and the STM tip become apparent: the bundles were repelled from the tip (set **A** of images in Fig. 5) when subjected

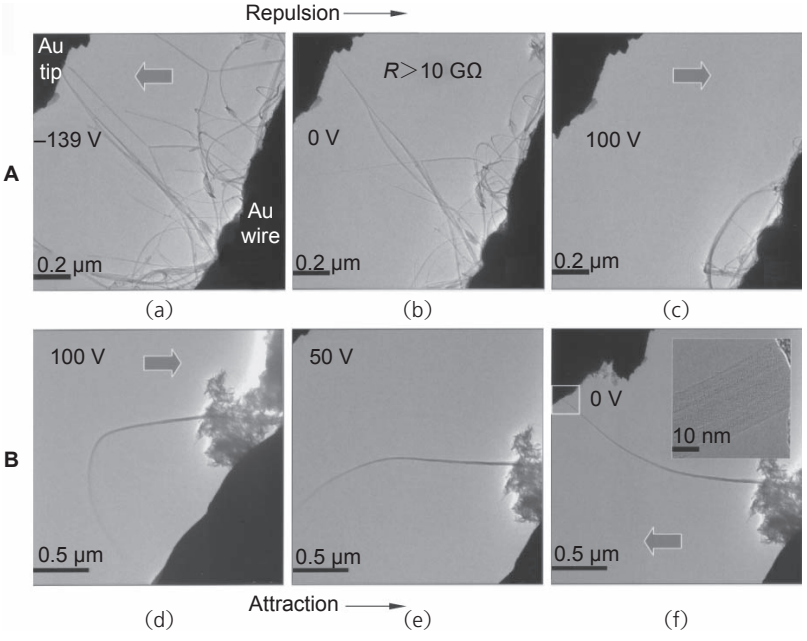

Figure 5 TEM images (a)–(f) showing the behavior of several thin, few-walled boron nitride nanotube bundles subjected to a gradient electric field along their lengths. The set of images **A** corresponds to the tube repulsion mode (under forward (+) tip biasing), whereas the set **B** illustrates the attraction mode (under reverse (–) tip biasing). The inset in (f) displays the structural details of an individual bundle

to forward potential (+) and attracted back to it whenever the polarity was reversed (−). This effect may be repeatedly used to manipulate the position of the bundle between the electrodes. These results are in agreement with our previous observations on magnesium-oxide and magnesium peroxide-filled multi-walled boron nitride nanotubes [12].

2.2.2 *Individual pure well-structured multi-walled boron nitride nanotubes*

Similar to the above-mentioned case, these nanotubes did not reveal any current up to very high voltages, indicating that they remained fully insulating. However, due to electrostatic interactions, the tube could be easily (and repeatedly) bent in an instantaneous fashion, much like a switch, as illustrated in Figs. 6(a)–(d). When the tip bias voltage was swept from +60 V to −60 V, the tube elastically bent upwards. The direction of tube bending could then be manipulated (i.e., a downward movement) by a simple reversal of polarity.

2.2.3 *Organic moiety-functionalized boron nitride nanotubes*

In contrast to the pure boron nitride nanotubes discussed above, these materials were found to conduct at relatively high voltage. The electrical breakdown occured at potential differences of several tens of volts (Fig. 7), and varied from tube to tube, perhaps reflecting the quality of the organic moiety (polyvinylpyrrolidone, PVP) surface layer. Discrete surface coverage might be responsible for the higher overall resistances, which, in general, were found to be in the range 20–40 MΩ. The *I*–*V* curves were characteristic of a Schottky-type semiconductor. The measured currents through the structures, just after the tube electrical breakdown, were in excess of 500

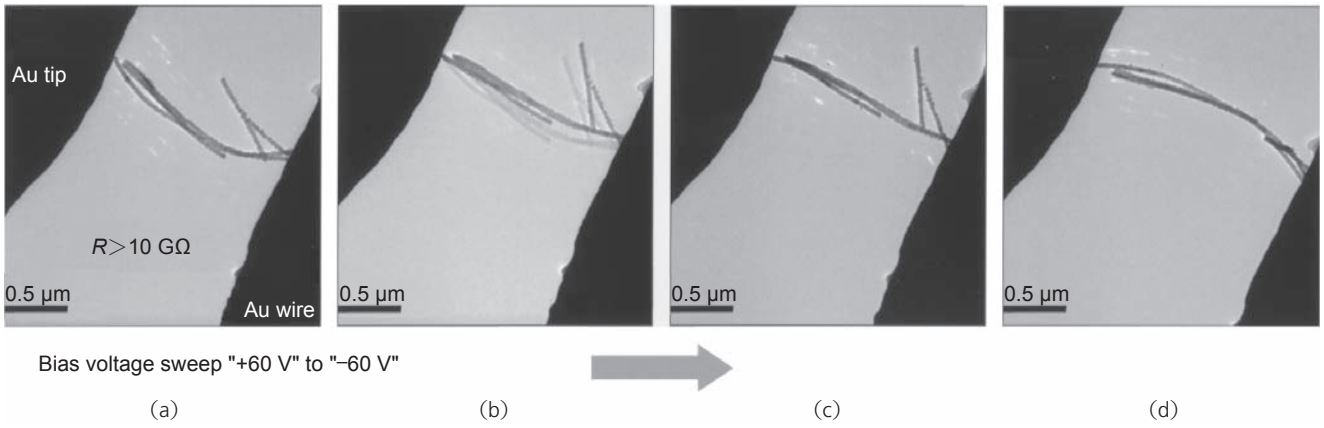

Figure 6 Consecutive TEM images (a)–(d) depicting the switch-like bending action experienced by an ensemble of individual multi-walled boron nitride nanotubes under bias sweeping. This phenomenon is due to the initial tube charging in TEM coupled to fast bias changes from 0 V to +60 V and then back to −60 V

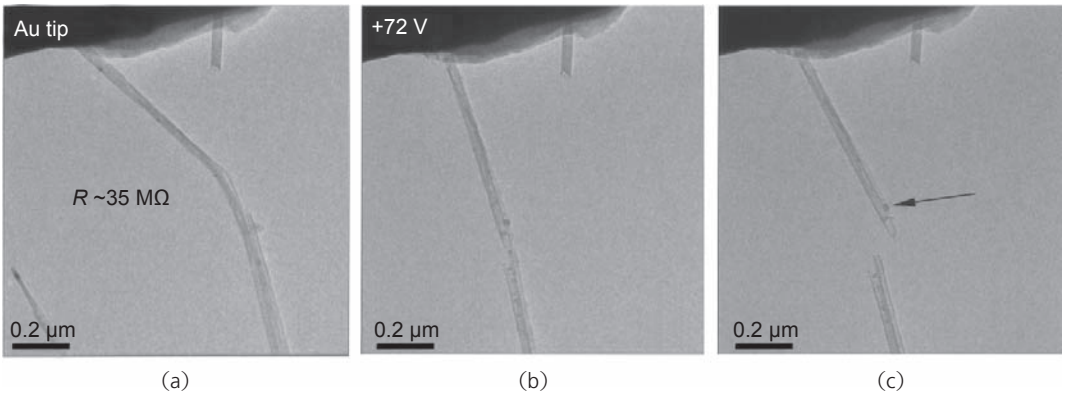

Figure 7 TEM images (a)–(c) demonstrating the structural failure of a carbon-functionalized multi-walled boron nitride nanotube under high bias voltage (+72 V) on the gold tip. The broken fragments reveal dark-contrast balls, presumably corresponding to amorphous carbon phases originating from the initial surface grafted material

nA. When steady flows of high current densities were delivered, significant morphological changes took place within the tubes for bias voltages above +30–40 V. The tubes gradually started to melt and eventually failed in the presence of a bias of ~70 V, leaving irregularly-shaped particles deposited on both the internal and external surfaces of the broken nanotubes. It is assumed that these are the remains of decomposed organic moieties destroyed by the combined action of the electron beam and current-induced tube heating.

3. Discussion

The data obtained in the present work are summarized in Table 1. The key feature of our experiments is that all measurements were performed using an identical setup, with the same electrode material (gold), nanotube sample procedure loadings, range of bias voltage windows and imaging conditions. Therefore, the different systems can be directly compared as regards their failure behaviors under high current flows.

The stability of the carbon nanotubes to the electrical current flow was found to depend on the degree of structural order. For the three tube types studied, those with higher densities of defects (fibers) showed lower ranges of failure voltage (4 –7 V). In contrast, the double-walled and multi-walled nanotubes showed similar tolerances (±7 –8 V) which implies that the number of walls is not significant. All the tubes showed well-defined metallic character when firmly contacted between the two gold terminals. Prior to their structural collapse, the carbon nanotubes/nanofibers withstand and may carry current densities of ~10^6 A/cm^2 or more. Catastrophic failure always starts from the outermost layers and proceeds inwards, mostly occurring in the mid-length region of the tube, relatively far from the contact points. This process results in the gradual thinning of the nanotubes. The result shown in Figs. 6 and 7, provide compelling evidence of a diffusive conduction mechanism. It is expected that for the case of two-probe systems like the one employed here, the path of least resistance for the current conduction will be through the outer layers of the nanotubes. However, it is also known that interlayer charge transport will take place at high bias due to the action of thermally activated carriers responsible for the gradual thinning [23]. Interestingly, the process of layer-by-layer failure is not accompanied by increasing disorder of the tubular structure. This is in line with recent theoretical modeling studies highlighting the role of pentagon–heptagon ring reorganizations in preserving the tube identity and a quasi-flawless tube shrinking under thermal heating or high-energy particle irradiation [24]. The carbon atoms are believed to enter the gas phase from the pentagon–heptagon dislocation cores under a substantial Joule heating-induced layer sublimation.

The high-resolution TEM structural imaging of the carbon nanotube was rather challenging because they represent free-standing protruding cantilevers prone to electron-beam charging effects with corresponding drifting and blurring under the electron irradiation. Nonetheless, it was possible to observe that the broken double-walled carbon nanotube ends consist of several tubes as opposed to individual tubular structures and/or graphitic layers (Fig. S-1). The numerous electrode-nanotube contact points and interconnections between entangled bundles, as evidenced by TEM (Fig. 2), may explain the very high values of resistance observed (Table 1).

Carbon nanotube degradation during two-probe measurements has also been reported by other groups [25–28]. During SEM observations Collins et al. [25] observed that arc-discharged nanotubes were degraded shell by shell and every outermost conducting wall failed at 10–100 μA. Suzuki et al. [28] studied herringbone-like carbon fibers (similar to the disordered carbon fibers used in this work) in an SEM with scanning TEM (STEM) capability and reported currents reaching 2060 μA at ~4.8 V.

In particular for two-probe systems, measurements of degradation currents depend on several important variables. Even considering the simplest case of an Ohmic circuit, where $I = \int(1/R)\mathrm{d}V$, the resistance R may still change considerably due to the nature of the contacts (Fermi alignment and/or chemical stability) or even structure bending. In contrast, the voltage V is independently controlled by the electronics of the holder, and therefore not subjected to changes

Table 1 Electrical parameters and structural response of various types of carbon and boron nitride nanotubes to a gradient electric field created by the in situ TEM nanotube biasing

System	Tube type	Electrical resistance (kΩ)	Electrical breakdown voltage (V)	Physical failure voltage (V)	Behavioral comments
Carbon	Double-walled nanotube bundles	$(\sim 1–2) \times 10^3$	~1–2 (bunch) Metallic (single)	~9	Gradual bundle unraveling
	Individual arc-discharge nanotubes	$(\sim 1.8–2) \times 10^2$	Metallic	~8–10	Consumption from outer layers
	Plasma-enhanced CVD-grown fibers	$\sim 6 \times 10^2$	Metallic	~4–7	Gradual fiber thinning to from single graphene sheet
Boron nitride	Few-walled nanotube bundles	$> 10^7$	>140	>140	Bundle repulsion / attraction under polarity change
	Individual multi-walled nanotubes	$>10^7$	>140	>140	Switch-like action under polarity change
	Carbon functionalized multi-walled nanotubes	$(\sim 20–60) \times 10^3$	~20–40	~70	Burning with residue of graphitic balls

in the electrode-nanostructure-electrode settings. Insofar as the present work dwells on the comparison of nanotubular structures with varying levels of order, chemistry, diameter and lengths, bias voltage values are reported instead of degradation currents. However, as most previous studies quote current values, these were also estimated. Not considering the double-walled nanotube case (due to the above-mentioned difficulties in obtaining the individual tube conductance), degradation currents at the failure voltages (Table 1) were in the range 50–60 μA for the arc-discharge tubes and 7–11 μA for the CVD-grown fibers. The former values are in good agreement with the data of Collins [25] and Wei [27] for well-structured carbon nanotubes, but the latter are significantly lower than those previously reported for disordered carbon fibers [28]. This may be due to structural differences such as the initial narrowness of the void tubular core of the materials used in this work. The effects of resistive heating during electrical current flow through a system of three resistors (two tube-gold contact areas plus the tube itself) can be quantified [26, 27] for strictly cylindrical conductors of known thermal conductivity and resistivity, which is definitely not the case for the above materials. In fact, the measured values of thermal conductivities and resistivities of carbon nanostructures may vary over an incredibly wide range depending on factors such as cross-sectional types, conducting paths, contact resistances, and defect status. A large number of these parameters remain unknown making such calculations impossible. The drastic rise in tube temperatures (up to 3500 K) [27] caused by Joule heating results in their degradation by carbon atom sublimation from the tube mid-length regions (Figs. 3 and 4).

Regarding the boron nitride nanotube systems, it should be noted that in the absence of significant flattening deformations [14] or doping levels [29] these nanomaterials represent a perfect insulator with an overall resistance exceeding ~10 GΩ. The dielectric character leads to boron nitride nanotube charging inside TEM (typically the boron nitride nanotubes are positively charged) which stimulates

strong electrostatic interactions between the biased STM tip and the nanostructures. It was found that these phenomena were particularly useful in that they facilitate the delicate adjustment of the tube position inside the TEM prior to further manipulation and electromechanical probing. Extensive functionalization of the boron nitride nanotubes with PVP results in surface grafting with a graphitic-like layer. This explains the observation of electrical conduction with current flows reaching several hundreds of nanoamperes at electrical breakdown voltages of ~30 V. Not surprisingly, the current density remains relatively low and does not exceed 10^4 A/cm^2. Furthermore, structural failure takes place rather abruptly, without the gradual shrinkage peculiar to the carbon systems, as shown in Fig. 7. The broken edges resemble the result of a sharp mechanical cut, while the diameter of the tubes remains nearly unchanged at the failure point. The remains of the functionalized surface groups are typically visible at the broken edges in the shape of corrugated dark-contrast balls. The unexpected failure of these boron nitride nanotubes, otherwise capable of withstanding harsher conditions than their carbon counterparts, is clearly a consequence of their functionalization. It is proposed that the capability of the outer carbon-containing layers to conduct current allied to the highly resistive nature of boron nitride leads to the activation of temperature dependent carriers and possible boron nitride interlayer tunneling. Temperatures in excess of 3273 K (the melting point of boron nitride is 3246 K) are known to occur for these high bias experiments as a result of Joule heating and this may be responsible for the catastrophic failure of the nanotubes.

4. Summary

Comparative evaluation of the electrical behavior for the two most competitive nanotube systems, namely carbon and boron nitride, was undertaken using the same experimental STM–TEM setup. Electrical failure of carbon nanotubes takes place at bias voltages approaching ±7 V whereas fibers are destroyed within the range 4–7 V. Prior to the physical failure of a nanotube and/or nanotube bundle, its diameter gradually shrinks, notably in its middle region, leaving only a few, or occasionlly, a single graphitic layer (graphene) as remainder.

Multi-walled boron nitride nanotubes were found to be much more robust to electrical breakdown and physical failure, withstanding voltages of up to ±140 V without significant changes in their structure. Electrostatic interactions between the oppositely charged setup fragments are of prime importance in these systems. Surface functionalization, along with tube doping, could be an elegant strategy to modify the insulating properties of boron nitride and give more highly conducting structures withstanding intermediate bias voltage regimes of up to ±70 V. After electrical breakdown of such functionalized boron nitride nanotubes, at around ±20–40 V, the current density remains relatively low and at least two orders of magnitude lower than that in the carbon nanotube systems.

Acknowledgements

The authors are indebted to Drs. M. Endo, Y. Ando, and K. Klein for providing double-walled, multi-walled, and disordered carbon nanostructures, respectively, and to Dr C. Y. Zhi for preparing the functionalized boron nitride samples employed in this study. The technical support of Mr. K. Kurashima and Dr. O. Lourie is also appreciated. This work was financially supported by the Nanoscale Materials Center Project, and, in part, by the World Premier International Center for Materials Nanoarchitectonics (MANA) Project, both tenable at the National Institute for Materials Science (NIMS).

Electronic Supplementary Material: Supplementary material is available in the online version of this article at http://dx.doi.org/10.1007/s12274-008-8010-y and is accessible free of charge.

References

[1] Gao, J.; Wang, Q.; Dai, H. J. Electron transport in very clean, as grown suspended carbon nanotubes. *Nat. Mater.* **2005**, *4*, 745–749.

[2] Avouris, P. Electronics with carbon nanotubes. *Phys.*

World **2007**, *20*, 40–45 (and references therein).

[3] Cumings, J.; Collins, P. G.; Zettl, A. Materials—peeling and sharpening multiwall nanotubes. *Nature* **2000**, *406*, 586.

[4] Svensson, K.; Olin, H.; Olsson, E. Nanopipettes for metal transport. *Phys. Rev. Lett*. **2004**, *93*, 145901.

[5] Cumings, J.; Zettl, A. Field emission and current-voltage properties of boron nitride nanotubes. *Solid State Commun*. **2004**, *129*, 661–664.

[6] Huang, J. Y.; Chen, S.; Jo, S. H., Wang, Z, Han, D. X., Chen, G.; Dresselhaus, M. S.; Ren, Z. F. Atomic-scale imaging of wall-by-wall breakdown and concurrent transport measurements in multiwall carbon nanotubes. *Phys. Rev. Lett*. **2005**, *94*, 236802.

[7] Wang, M. S.; Chen, Q.; Peng, L.-M. Grinding a nanotube. *Adv. Mater*. **2008**, *20*, 724–728.

[8] Wei, X. L.; Chen, Q.; Liu, Y., Peng, L.-M. Cutting and sharpening carbon nanotubes using a carbon nanotube nanoknife. *Nanotechnology* **2007**, *18*, 185503.

[9] Sawaya, S.; Akita, S.; Nakayama, Y. Correlation between the mechanical and electrical properties of carbon nanotubes. *Nanotechnology* **2007**, *18*, 035702.

[10] Suekane, O.; Nagataki A.; Nakayama, Y. Current-induced curing of defective carbon nanotubes. *Appl. Phys. Lett*. **2006**, *89*, 183110.

[11] Cumings, J.; Olsson, E.; Petford-Long, A. K.; Zhu, Y. M. Electric and magnetic phenomena studied by in situ transmission electron microscopy. *MRS Bull.* **2008**, *33*, 101–106.

[12] Golberg, D.; Mitome, M.; Kurashima, K.; Zhi, C. Y.; Tang, C. C.; Bando, Y.; Lourie, O. *In situ* electrical probing and bias-mediated manipulation of dielectric nanotubes in a high-resolution transmission electron microscope. *Appl. Phys. Lett*. **2006**, *88*, 123101.

[13] Golberg, D.; Costa, P. M. F. J.; Mitome, M.; Mueller, Ch.; Hampel, S.; Leonhardt, A.; Bando, Y. Copper-filled carbon nanotubes: Rheostatlike behavior and femtogram copper mass transport. *Adv. Mater*. **2007**, *19*, 1937–1942.

[14] Bai, X. D.; Golberg, D.; Bando, Y.; Zhi, C. Y.; Tang, C. C.; Mitome, M.; Kurashima, K.; Deformation-driven electrical transport of individual boron nitride nanotubes. *Nano Lett.* **2007**, *7*, 632–637.

[15] Costa, P. M. F. J.; Golberg, D.; Mitome, M.; Bando, Y. Nitrogen-doped carbon nanotube structure tailoring and time-resolved transport measurements in a transmission electron microscope. *Appl. Phys. Lett*. **2007**, *91*, 223108.

[16] Costa, P. M. F. J.; Golberg, D.; Mitome, M.; Bando, Y. Electrical properties of CN_x nanotubes probed in a transmission electron microscope. *Appl. Phys. A—Mater.* **2008**, *90*, 225–229.

[17] Kim, Y. A.; Muramatsu, H.; Hayashi, T.; Endo, M.; Terrones, M.; Dresselhaus, M. S. Fabrication of high-purity, double-walled carbon nanotube buckypaper. *Chem. Vap. Depo.*, **2006**, *12*, 327–332.

[18] Ando, Y.; Iijima, S. Preparation of carbon nanotubes by arc-discharge evaporation. *Jpn. J. Appl. Phys*. **1993**, *32*, L107–L109.

[19] Melechko, A. V.; Merkulov, V. I.; McKnight, T. E., Guillorn, M. A.; Klein, K. L.; Lowndes, D. H., Simpson, M. L. Vertically aligned carbon nanofibers and related structures: Controlled synthesis and direct assembly. *J. Appl. Phys*. **2005**, *97*, 041301.

[20] Golberg, D.; Bando, Y.; Kurashima, K.; Sato, T. Ropes of BN multi-walled nanotubes. *Solid State Commun*. **2000**, *116*, 1–6.

[21] Zhi, C. Y.; Bando, Y.; Tang, C. C.; Golberg D. Effective precursor for high yield synthesis of pure BN nanotubes. *Solid State Commun*. **2005**, *135*, 67–70.

[22] Zhi, Y. C.; Bando, Y.; Tang, C. C.; Kuwahara, H.; Golberg D. Grafting boron nitrides: From polymers to amorphous and graphitic carbon. *J. Phys. Chem. C* **2007**, *111*, 1230–1233.

[23] Collins, P. G.; Hersam, M.; Arnold, M.; Martel, R.; Avouris, Ph. Current saturation and electrical breakdown in multiwalled carbon nanotubes. *Phys. Rev. Lett*. **2001**, *86*, 3128–3131.

[24] Ding, F.; Jiao, K., Lin, Y.; Yakobson, B. I. How evaporating carbon nanotubes retain their perfection. *Nano Lett*. **2007**, *7*, 681–684.

[25] Collins, P. G.; Avouris, P. Multishell conduction in multiwalled carbon nanotubes. *Appl. Phys. A—Mater.* **2002**, *74*, 329–332.

[26] Bonard, J.-M.; Klinke, C.; Dean, K.A.; Coll, B.F. Degradation and failure of carbon nanotube emitters. *Phys. Rev. B* **2003**, *67*, 115406.

[27] Wei, W.; Liu, Y., Wei, Y.; Jiang, K.; Peng, L.-M.; Fan, S. Tip cooling effect and failure mechanism of field-emitting carbon nanotubes. *Nano Lett*. **2007**, *7*, 64–68.

[28] Suzuki, M.; Ominami, Y.; Ngo, Q.; Yang, C. Y. Current-induced breakdown of carbon nanofibers. *J. Appl. Phys*. **2007**, *101*, 114307.

[29] Golberg, D.; Bando, Y.; Tang, C. C.; Zhi, C. Y. Boron nitride nanotubes. *Adv. Mater*. **2007**, *19*, 2413–2432.